Kuss, Alexander ; Ksensow, Konstatin ; Verl, Alexander
Deformable shape registration using surface-based free-form deformations in robotic welding
In: 2017 IEEE/ASME International Conference on Advanced Intelligent Mechatronics : 3-7 July 2017, Munich, Germany. - Piscataway: IEEE, 2017, S. 885-890. DOI: 10.1109/AIM.2017.8014130

Deformable Shape Registration Using Surface-Based Free-Form Deformations in Robotic Welding

Alexander Kuss[1], Konstantin Ksensow[2], Alexander Verl[3]

***Abstract*— In this paper, a novel approach is presented to perform a deformable shape registration of workpiece geometries in robotic welding. Based on the free-form deformation (FFD) method, a surface-based extension FFDS is presented where the initial shape of the control points lattice corresponds to the shape of the surface to be deformed. A point-based registration is performed using the sum of least squares criteria to obtain the non-rigid shape transformation. The deformation is applied to the computer-aided design (CAD) model of the workpiece geometry preserving its topology for subsequent robot path planning to move a welding gun along the deformed part contours. The performance of the presented approach is evaluated using virtual test data and real measurements of a welding workpiece obtained with a 3D sensor. Moreover, the performance of this approach is compared to state of the art deformable shape registration revealing a significant reduction of computation time and the usability for path planning in robotic welding.**

I. INTRODUCTION

Robotic welding systems are widely used in the manufacturing industry. However, in small and medium sized enterprises (SMEs) with small lot sizes and uncertain production environments, cost-effective automation of welding processes is still a challenge [1]. Especially, the programming of the robot system for new parts can be a time-consuming and expert-dependent task that obstructs the usage of robots in these production scenarios. Research in this field falls into two categories: online and offline programming [2]. In online programming, the operator moves the robot end effector to different positions using a teach pendant. The sequence of teached points and additional process-related commands represent the final robot program. Even though online programming is simple and widespread in industry, it can be time-consuming for complex workpiece geometries and leads to downtimes of the robot system. Moreover, the quality of the robotic welding process depends on the expertise of the human programmer.

To overcome these drawbacks, offline programming (OLP) systems can be used. Based on a 3D simulation of the robot cell, the robot movement can be virtually programmed along the contours of the 3D CAD model of the workpiece. To adapt the location of the CAD part to the real workpiece, some approaches focus on a precise object localization based on optical [3] or tactile [4] sensing. However, due to manufacturing inaccuracies, there might also be geometric variations between CAD model and the actual weld part. It is a fundamental problem in robot program planning based on CAD models that these variations might be beyond acceptable limits for a correct execution of the welding process.

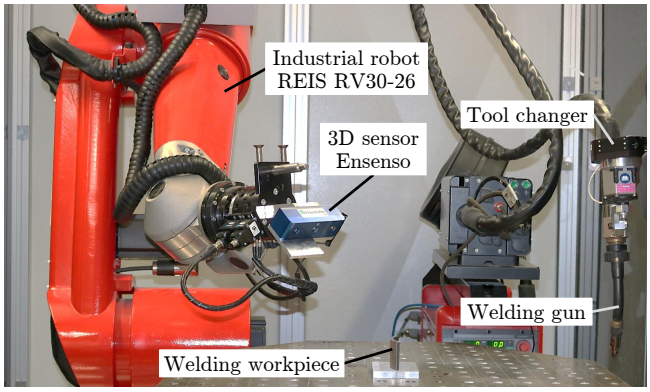

Fig. 1. Setup of robotic welding system with 3D sensor to measure workpiece shape deformations

II. RELATED WORK

Several approaches focus on tracking of the joint contours based on 2D laser sensors and real-time adaptation of the robot path [5], [6]. However, the adaptation strategy has to be reconfigured for each new part geometry and is limited to simple workpiece geometries. Other approaches focus on computer vision to reconstruct the entire geometry of the part based on 3D sensor data [7], [8]. Geometry reconstruction however needs complex computations and discards important CAD data information, like e.g. topology of a welding assembly. Another approach uses 3D sensor measurements to detect assembly variations due to inaccurate relative part positioning in a welding assembly and adapts its CAD model accordingly for subsequent offline robot path planning [9]. However, shape deviations of the single parts are neglected.

Registering of deformable objects can be achieved by extended shape deformation models with differential geometric constraints [10], [11]. In these approaches however, the deformation process has to be observed and it is not possible to adapt a CAD model to an already deformed shape of a

*The research leading to these results has received funding from the European Union's Horizon 2020 research and innovation program under grant agreement no. 688217 in the project ROBOTT-NET.

[1]Alexander Kuss is with Fraunhofer Institute for Manufacturing Engineering and Automation IPA, Nobelstrasse 12, 70569 Stuttgart, Germany. All correspondence should be addressed to Alexander Kuss alexander.kuss@ipa.fraunhofer.de

[2]Konstantin Ksensow is with University of Applied Sciences, Schellingstr. 24, 70174 Stuttgart, Germany

[2]Alexander Verl is with Institute for Control Engineering of Machine Tools and Manufacturing Units ISW, University of Stuttgart, Seidenstrasse 36, 70174 Stuttgart, Germany

workpiece geometry. Other approaches apply finite element methods (FEM) to integrate the parts' physical behavior into the registration process [12], [13], which however requires complex models and intensive computations.

Other approaches use free-form deformations (FFD) introduced by Sederberg et al. [14] as a basis for a non-rigid registration. The basic idea of FFD is to deform an object geometry by manipulating a lattice of control points containing the object. An extention of the FFD method to user-defined control lattices in the context of object design is proposed in [15]. Hsu et al. presented an approach to use FFD methods by manipulating the shape of an object directly which builds the basis for using FFD in non-rigid registration [16]. Much of the work in non-rigid registration based on FFD methods is done in the field of medical image registration [17], [18] using intensity-based methods. However, if landmarks are used in image registration approaches, they can also be used for point-based registration of geometry models represented as CAD data. A landmark-based image registration for 2D images using FFD with hierarchical B-Splines is presented in [19]. A similar approach is presented in [20], which is also applied to registration of 3D polygonal mesh data for face scan matching. In [21], a point-based registration of 2D images using FFD is presented. By introducing a linear system of control points, the size of the resulting matrix only depends on the size of the control point lattice improving computational efficiency. However, in all these approaches the deformed object is entirely enclosed by the control lattice of the FFD leading to a high number of control points and respective computational efforts to compute the deformations.

In this paper, a novel approach is proposed to perform a deformable shape registration based on a surface-based extension of the FFD method. It can be applied to CAD model geometries preserving topology information for subsequent robot path planning on welding parts.

This paper is structured as follows: In Section III, the approach for surface-based free-form deformation is presented. Section IV presents the validation of the proposed approach using virtual sensor data. Moreover, a validation is performed using sensor measurements of a real welding workpiece. Finally, conclusions are presented in Section V.

III. APPROACH

A. General concept for robot program planning based on deformable shape registration

The overall concept for robot program planning based on deformable shape registration is shown in Fig. 2 and consists of three main steps:

In step 1, a 3D point cloud is generated from the nominal CAD model of a product geometry. The resulting point cloud and a 3D sensor measurement of the real product geometry are used to perform a rigid and global registration. This is done by using point cloud matching based on the iterative closest point (ICP) method as presented in the authors' previous work [9], but is not focus of this paper. In step 2, point clouds are generated for each surface of the product geometry. A surface-based deformable registration is performed for each of these surfaces to account for local deformations and to generate an updated CAD model of the welding assembly. Finally in step 3, this updated CAD model is used as an input for robot program planning.

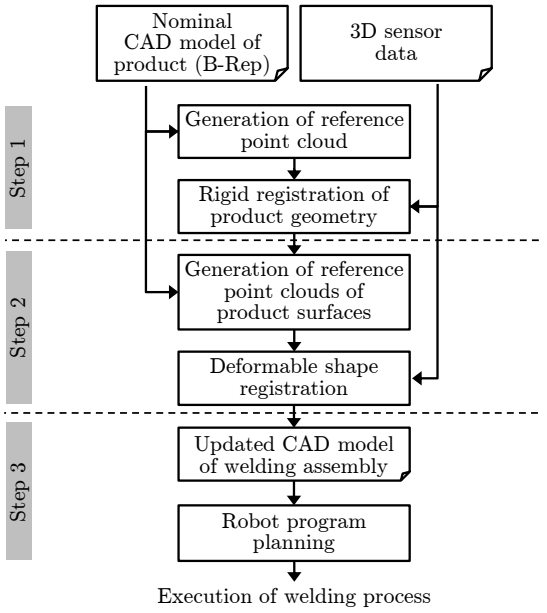

Fig. 2. Overall concept for robot program planning based on rigid and non-rigid registration

The focus of this paper is on the deformable shape registration in step 2, which is detailed in the following.

B. Deformable shape registration using surface-based FFD

The objective of deformable shape registration is to compute a deformation function that matches corresponding points of a source and a target point cloud. The source point cloud can be derived from a parameteric surface of the objects' CAD model, whereas the target point cloud can be obtained by measurements of the corresponding surface on a real workpiece. Let $S = \{\vec{s}_q\}$ be the source point cloud and $T = \{\vec{t}_r\}$ be the target point cloud with the points $\vec{s}_q$ and $\vec{t}_r$ in 3D space for $q = 1, ..., N_q$ and $r = 1, ..., N_r$. To perform a non-rigid registration for S and T, a local deformation field $L(p)$ using space warping models can be applied. We choose the free-form deformation method (FFD) based on B-splines introduced by Sederberg et al. [14] that enables shape deformation by manipulation of a grid of control points. In order to deform a 3D shape with FFD methods, a rectangular 3D grid of control points is applied enclosing the entire shape [22] as shown in Fig. 3 (a). Let $P = P_{i,j,k}$ be the control lattice with $i = 0, ..., N_i - 1$, $j = 0, ..., N_j - 1$ and $k = 0, ..., N_k - 1$ enclosing the source shape. In the initial rectangular configuration without deformation, the control lattice is denoted as P^0 and in the deformed configuration as $P = P^0 + \Delta P$. Supposing a deformation of the control point lattice from P^0 to P, the deformation of any point $p = s_q = (x, y, z)$ of the source point cloud S can be

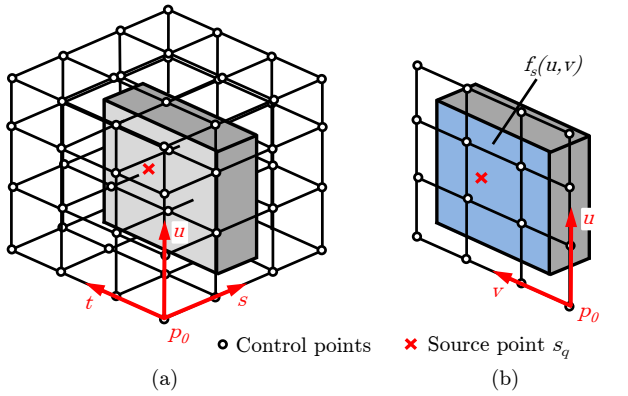

Fig. 3. Deformation of object geometry in 3D space using (a) FFD with 3D control point lattice and (b) FFDS with surface-based control point lattice

represented by a deformation using cubic B-splines (with order 4) of the following form:

$$L(p) = \sum_{i=0}^{l} \sum_{j=0}^{m} \sum_{k=0}^{n} N_{i,4}(s) N_{j,4}(t) N_{k,4}(u) P_{i,j,k} \quad (1)$$

where $l = N_i - 1$, $m = N_j - 1$ and $n = N_k - 1$. Here, $s, t, u \in [0, 1]$ are the parameters of p in the B-spline volume segment defined by the 3D-control lattice. $N_{i,4}(s)$, $N_{j,4}(t)$ and $N_{k,4}(u)$ represent the respective normalized cubic B-spline functions. In this case, the deformation of any point p is a linear function of 64 control points [16]. Using a fine resolution of the control point lattice, this may lead to high computation times. Moreover, the rectangular grid of control points enclosing a single face of the product geometry may result in many points that are not effected by the deformation, but have to be included in the calculation of $L(p)$.

Thus, we propose an approach for deformable shape registration using FFD methods with a different control point lattice, that is derived directly from the surfaces of the objects' CAD model. Fig. 3 shows the difference between state of the art FFD application with 3D control lattice (a) and the proposed approach using FFD with a surface-based control point lattice (b).

Let $\tilde{P}_{i,j}$ be the control point lattice with $i = 0, ..., N_i - 1$ and $j = 0, ..., N_j - 1$ that is defined in the source surface $f(u, v)$ with $u, v \in [0, 1]$ to be deformed. In the initial configuration without deformation, the control lattice $\tilde{P}_0$ can be obtained directly from the respective surface model of the boundary representation (B-rep) of the objects' CAD model. B-rep CAD data is widely-used in production and supported by various open exchange formats like i.e. STEP (see ISO 10303). The deformed configuration is then denoted as $\tilde{P} = \tilde{P}_0 + \Delta\tilde{P}$. Using cubic B-splines, the deformation of any point $p = s_q = (x, y, z)$ on the source surface is then represented by:

$$\tilde{L}(p) = \sum_{i=0}^{m} \sum_{j=0}^{n} N_{i,4}(u) N_{j,4}(v) \tilde{P}_{i,j} \quad (2)$$

where $m = N_i - 1$ and $n = N_j - 1$. The parameters u, v represent p within the B-spline surface. $N_{i,4}(u)$ and $N_{j,4}(v)$ are the normalized cubic B-spline functions. Here, the deformation of any point p only depends on 16 control points. From Equ. 2 the following matrix equation can be deduced to describe the difference Δp between the position of a point after the deformation compared to its initial position:

$$\Delta p = B \Delta \tilde{P} \quad (3)$$

However, in the case of deformable shape registration, the deformation is unknown, whereas point displacements are given. Hence, to solve for the deformation $\tilde{P}$, we use the pseudoinverse B^+ that represents an optimal least-square solution as detailed in [16], [23]:

$$\Delta \tilde{P} = B^+ \Delta p \quad (4)$$

The algorithm to obtain the deformation field that matches the source points S with the target points T involves the following steps:

1) Set the control lattice parameters N_i and N_j
2) Compute the control lattice
3) For each point in S determine its closest neighbour in T
4) Solve Equ. 4 to obtain the deformation
5) Apply the deformation on the source shape

As the deformation represents as a B-spline function, it can also be applied on all other elements that are defined in the original surface, like i.e. boundary curves and edges. This enables a direct adaptation of the original B-rep CAD model of the product according to the computed deformations.

IV. EXPERIMENTAL VALIDATION

The validation of the proposed approach is performed on a typical welding workpiece. Fig. 4 (a) shows the workpiece geometry without deformation and a weld seam contour. In Fig. 4 (b), the deformed workpiece and the effect on the weld seam contour is visualized.

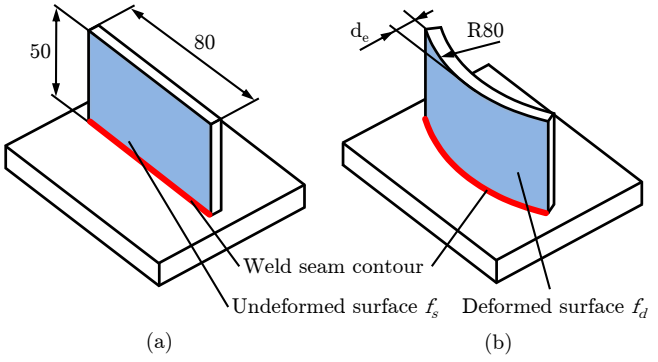

Fig. 4. Geometry of welding workpiece (a) without deformation and (b) with deformation

A. Virtual Test Case

In a first test case, virtual sensor data is used to perform an evaluation without additional influences, like e.g. sensor noise. To obtain virtual sensor data, a target point cloud T is generated on the deformed B-rep CAD surface f_d shown in Fig. 4 (b). The points of T are randomly distributed on the surface with an average point distance of $0.2\,\mathrm{mm}$ which corresponds to the resolution of the optical 3D sensor in the real robot system presented in Fig. 1.

The source points S are generated on the undeformed surface f_s of the objects' B-rep CAD model indicated in Fig. 4 (a). A uniform grid is used with equidistant points. In this test case, f_s is a plane surface. However, the approach can also be applied to other surface types, like i.e. cylindrical or B-spline surfaces.

The focus of the experimental validation is to evaluate the performance of the proposed FFDS approach for different numbers of source points and control points. The performance indicators are calculation time and matching accuracy. Calculation times are measured for computations performed with an Intel quad-core processor 2.8 GHz and 16 GB RAM. To measure the matching accuracy, an additional point cloud M is generated on the undeformed surface f_S with random point distribution and an average point distance of $0.2\,\mathrm{mm}$. After applying the calculated deformation on M, corresponding points in T are computed using k-d tree search. The resulting average Euclidean point distance represents a measure for the matching accuracy. Fig. 5 (a) shows the source point cloud S with 36 points, the target point cloud T with 104,705 points and the control point lattice with 25 control points without deformation. Moreover, a polygonal mesh of the undeformed surface f_s is displayed. In Fig. 5 (b), the resulting control lattice deformation after calculation of the FFDS is visualized as well as the applied deformation on the original surface and on the point cloud M.

The results of the proposed approach are compared to a state of the art FFD algorithm by Hsu et al. [16] (FFD-HSU) that uses a 3D control point lattice as indicated in Fig. 3 (a).

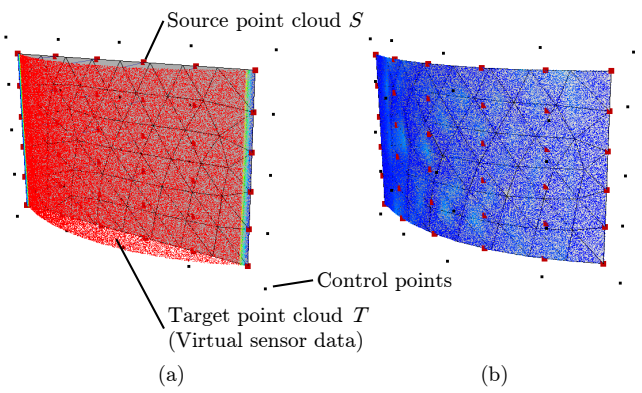

Fig. 5. Visualization of virtual sensor data T, source point cloud S and control point lattice of FFDS (a) before deformation and (b) after deformation

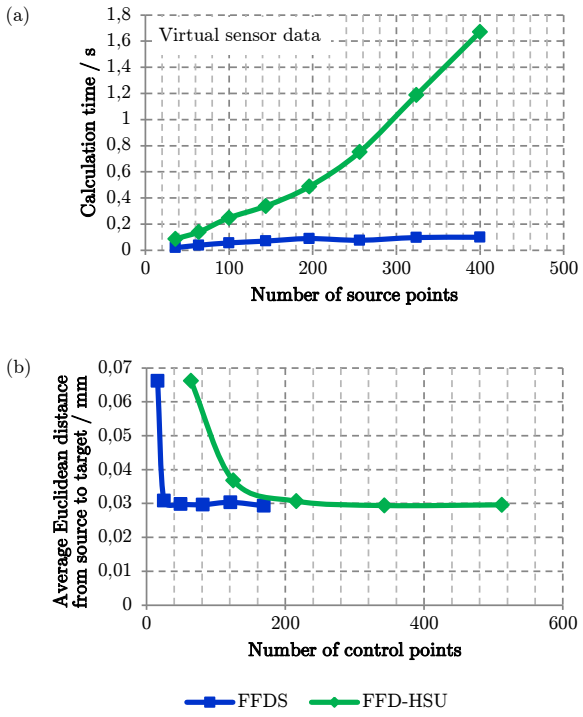

Fig. 6. Evaluation of (a) calculation times depending on the number of source points for $N = 10$ control points per spatial direction for virtual sensor data and (b) matching accuracy depending on number of control points for 400 source points for virtual sensor data

We assume an equal number of control points per spatial direction $N = N_i = N_j = N_k = N_m = N_n$. Fig. 6 (a) shows the results of calculation times depending on the number of source points for $N = 10$. The FFDS approach shows a linear regression of calculation times, whereas the FFDS-HSU algorithm indicates an exponential regression of calculation time with increasing number of control points. In the case of using 400 source points, the calculation time decreases from 1.67 seconds with the FFD-HSU approach to 0.10 seconds with the proposed approach.

Moreover, Fig. 6 (b) shows the influence of the number of control points on the matching accuracy represented by the average Euclidean distance between M and T after the deformation. Using a constant number of 400 source points, the results reveal a stable matching accuracy of around $0.03\,\mathrm{mm}$ for a minimum of 25 control points with the FFDS approach. The same accuracy with the FFD-HSU approach is only reached starting from a minimum of 216 control points.

B. Test Case with Real Measurement Data of a Welding Workpiece

The proposed approach is also validated with a real robotic welding system shown in Fig. 1. The end effector of the 6-axis industrial robot is equipped with a 3D stereo camera to measure the workpiece geometry. The 3D camera provides a point cloud of maximum 360,000 points per measurement and has an optimum x-y view field of $155 \times 118\,\mathrm{mm}$, which corresponds to an average point distance of around

0.2 mm in the x-y plane. The z-accuracy of the sensor for a measurement distance of 370 mm is specified with 0.13 mm The evaluation is performed for a real welding workpiece made of non-alloy structural steel shown in Fig. 7. The dimensions correspond to the dimensions in the virtual test case as indicated in Fig. 4 (b).

Fig. 8 (a) shows the target point cloud T obtained from measurement of the real workpiece geometry including 42,087 points. Moreover, the source point cloud S with 36 source points and the control lattice with 25 control points without deformation are visualized. The resulting control point lattice deformation after computation of the FFDS and the deformation application on the original surface and the point cloud M is illustrated in Fig. 8 (b).

The focus of this validation is to evaluate the performance of the proposed FFDS approach for real measurement data. Therefore, as in Section IV-A, the influence of the number of source and control points on the calculation time and the matching accuracy is determined. The results are again compared to the results obtained by using the FFD algorithm by Hsu et al. [16] (FFD-HSU) with a 3D lattice of control points.

Fig. 9 (a) shows the results of the deformation computation for different numbers of source points and the respective calculation times. As in the test case for virtual sensor data, calculation times for the FFDS approach indicate a linear regression with increasing number of source points. In the

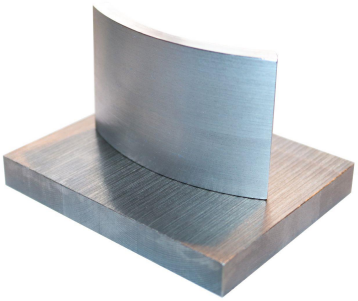

Fig. 7. Real welding workpiece with deformation

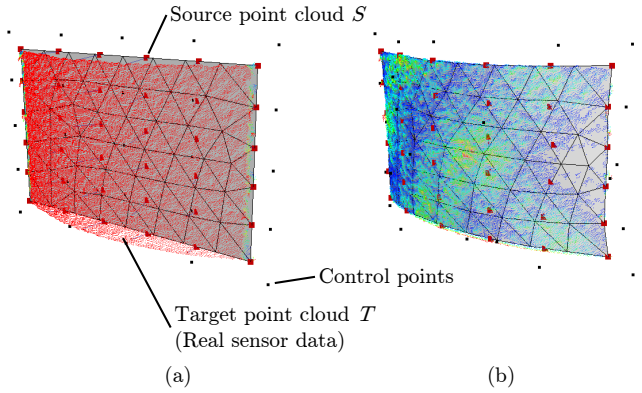

Fig. 8. Visualization of real sensor data T, source point cloud S and control point lattice of FFDS (a) before deformation and (b) after deformation

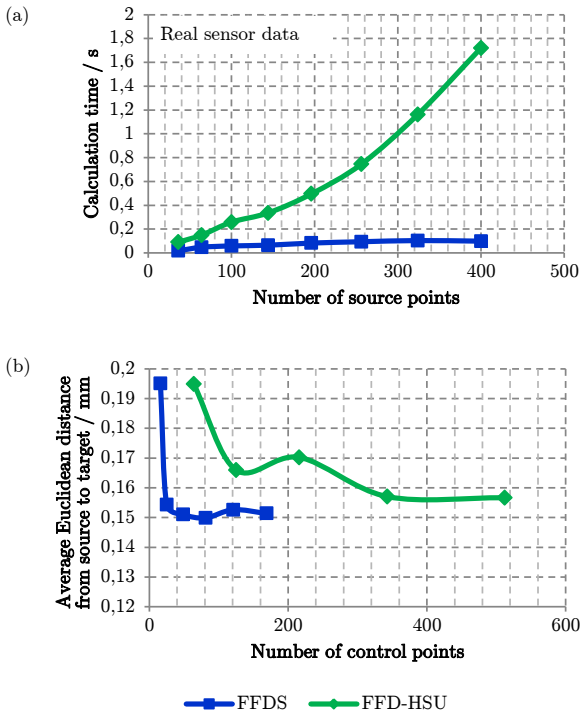

Fig. 9. Evaluation of (a) calculation times depending on the number of source points for $N = 10$ control points per spatial direction and (b) matching accuracy depending on number of control points for 400 source points for real sensor data

FFD-HSU case, the calculation times show an exponential regression for increasing source point numbers. Using 400 source points, the calculation time decreases from 1.69 seconds with the state of the art FFD approach to 0.10 seconds with the proposed approach. This indicates the benefits of the proposed approach in applications with a high number of point comparisons.

In Fig. 9 (b), the influence of the number of control points on the matching accuracy is evaluated assuming 400 source points. The results show a stable matching accuracy of around 0.15 mm for a minimum of 36 control points with the FFDS approach. In the FFD-HSU case with a 3D control point lattice, a minimum of 343 control points is needed to reach a stable matching accuracy. Moreover, in this case, the average Euclidean distance with around 0.16 mm is slightly higher than with the proposed approach.

V. CONCLUSION AND FUTURE WORK

In this paper, a novel approach has been proposed for deformable shape registration of workpiece geometries in robotic welding. The approach extends the free-form deformation (FFD) method by introducing a new control point lattice that is derived from the surfaces of the products' CAD model. Here, the parameterized surfaces are extracted directly from the boundary representation (B-rep) CAD model widely-used in production environments. A point-based registration is performed using the pseudoinverse for an optimal least-square solution. The resulting deformation

can be applied on the original B-rep CAD data, like surfaces, edges and points and hence preserves the topology of the original product model. This is decisive for a subsequent CAD-based robot programming.

The approach was validated using virtual sensor data as well as real sensor measurements from a welding workpiece. The results were compared to state of the art FFD with 3D control point lattice enclosing the entire product geometry model. Using the proposed approach and real measurement data, the calculation time for 400 source points was reduced from 1.69 to 0.10 seconds. Moreover, the same matching accuracy between source and target point cloud after deformation was reached with less control points. Using real sensor data, a matching accuracy of around $0.15\,\mathrm{mm}$ was reached with 36 control points, whereas with the conventional FFD method 343 control points were needed to reach a similar accuracy.

In particular for a high number of point correspondences, the proposed approach indicates its efficiency compared to conventional FFD registration. Additionally, the approach can be used in combination with state of the art CAD-based robot program planning. While preserving topological information, the approach allows to generate an updated B-rep CAD model including deformations to minimize shape variations between virtual model and real welding workpiece geometry.

Future work will focus on application of surface deformations on complete CAD models including edges and vertices. Moreover, the control lattice of the proposed approach will be applied on initially curved surfaces like cylindrical or B-spline surfaces.

REFERENCES

[1] A. Kuss, J. R. Diaz Posada, R. Hollmann, T. Dietz, and M. Haegele, "Manufacturing knowledge for industrial robot systems: Review and synthesis of model architecture," *12th IEEE Conference on Automation Science and Engineering*, 2016.

[2] Z. Pan, J. Polden, N. Larkin, S. Van Duin, and J. Norrish, "Recent progress on programming methods for industrial robots," *Robotics and Computer-Integrated Manufacturing*, vol. 28, no. 2, pp. 87–94, 2012.

[3] M. Rajaraman, M. Dawson-Haggerty, K. Shimada, and D. Bourne, "Automated workpiece localization for robotic welding," *IEEE International Conference on Automation Science and Engineering*, pp. 681–686, 2013.

[4] K. Suwanratchatamanee, M. Matsumoto, and S. Hashimoto, "Robotic tactile sensor system and applications," *IEEE Transactions on Industrial Electronics*, vol. 57, no. 3, pp. 1074–1087, 2010.

[5] R. Manorathna, P. Phairatt, P. Ogun, T. Widjanarko, M. Chamberlain, L. Justham, S. Marimuthu, and M. R. Jackson, "Feature extraction and tracking of a weld joint for adaptive robotic welding," *13th International Conference on Control Automation Robotics & Vision*, pp. 1368–1372, 2014.

[6] Z. Fang, D. Xu, and M. Tan, "A vision-based self-tuning fuzzy controller for fillet weld seam tracking," *IEEE/ASME Transactions on mechatronics*, vol. 16, no. 3, pp. 540–550, 2011.

[7] M. Dinham and G. Fang, "Weld seam detection using computer vision for robotic arc welding," *IEEE International Conference on Automation Science and Engineering (CASE)*, pp. 771–776, 2012.

[8] Z. Bi and B. Kang, "Sensing and responding to the changes of geometric surfaces in flexible manufacturing and assembly," *Enterprise Information Systems*, vol. 8, no. 2, pp. 225–245, 2014.

[9] A. Kuss, U. Schneider, T. Dietz, and A. Verl, "Detection of assembly variations for automatic program adaptation in robotic welding systems," *47th International Symposium on Robotics*, pp. 1–6, 2016.

[10] C. Papazov and D. Burschka, "Deformable 3d shape registration based on local similarity transforms," *Computer Graphics Forum*, vol. 30, no. 5, pp. 1493–1502, 2011.

[11] C. Kambhamettu, D. Goldgof, M. He, and P. Laskov, "3d nonrigid motion analysis under small deformations," *Image and Vision Computing*, vol. 21, no. 3, pp. 229–245, 2003.

[12] H. Zhong, J. Kim, H. Li, T. Nurushev, B. Movsas, and I. J. Chetty, "A finite element method to correct deformable image registration errors in low-contrast regions," *Physics in medicine and biology*, vol. 57, no. 11, p. 3499, 2012.

[13] A. Krol, M. Z. Unlu, A. Magri, E. Lipson, I. L. Coman, J. A. Mandel, K. G. Baum, and D. H. Feiglin, "Iterative finite element deformable model for nonrigid coregistration of multimodal breast images," *3rd IEEE International Symposium on Biomedical Imaging: Nano to Macro*, pp. 852–855, 2006.

[14] T. W. Sederberg and S. R. Parry, "Free-form deformation of solid geometric models," *ACM SIGGRAPH computer graphics*, vol. 20, no. 4, pp. 151–160, 1986.

[15] S. Coquillart, "Extended free-form deformation: a sculpturing tool for 3d geometric modeling," *Computer Graphics*, vol. 24, no. 4, 1990.

[16] W. M. Hsu, J. F. Hughes, and H. Kaufman, "Direct manipulation of free-form deformations," *Computer Graphics*, vol. 26, no. 2, pp. 177–184, 1992.

[17] D. Rueckert, L. I. Sonoda, C. Hayes, D. L. Hill, M. O. Leach, and D. J. Hawkes, "Nonrigid registration using free-form deformations: application to breast mr images," *IEEE transactions on medical imaging*, vol. 18, no. 8, pp. 712–721, 1999.

[18] T. Rohlfing, C. R. Maurer, D. A. Bluemke, and M. A. Jacobs, "Volume-preserving nonrigid registration of mr breast images using free-form deformation with an incompressibility constraint," *IEEE transactions on medical imaging*, vol. 22, no. 6, pp. 730–741, 2003.

[19] Z. Xie and G. E. Farin, "Image registration using hierarchical B-splines," *IEEE Transactions on Visualization and Computer Graphics*, vol. 10, no. 1, pp. 85–94, 2004.

[20] X. Huang, N. Paragios, and D. N. Metaxas, "Shape registration in implicit spaces using information theory and free form deformations," *IEEE transactions on pattern analysis and machine intelligence*, vol. 28, no. 8, pp. 1303–1318, 2006.

[21] H. Abdelmunim and A. A. Farag, "Elastic shape registration using an incremental free form deformation approach with the ICP algorithm," *Canadian Conference on Computer and Robot Vision (CRV)*, pp. 212–218, 2011.

[22] A. Sotiras, C. Davatzikos, and N. Paragios, "Deformable medical image registration: A survey," *IEEE transactions on medical imaging*, vol. 32, no. 7, pp. 1153–1190, 2013.

[23] T. L. Boullion and P. L. Odell, "Generalized inverse matrices," *Wiley*, 1971.